ICASE

ON MIXED FINITE ELEMENT METHODS

III. THE GRID DECOMPOSITION PROPERTY AND EXAMPLES

George J. Fix

Max D. Gunzburger

R. A. Nicolaides

Report Number 78-7

March 9, 1978

INSTITUTE FOR COMPUTER APPLICATIONS IN SCIENCE AND ENGINEERING

NASA Langley Research Center, Hampton, Virginia

Operated by the

UNIVERSITIES SPACE USRA RESEARCH ASSOCIATION

ON MIXED FINITE ELEMENT METHODS
III. The Grid Decomposition Property and Examples

George J. Fix*

Max D. Gunzburger†

R. A. Nicolaides#

ABSTRACT

The previous papers in the series have provided a theoretical framework for the Galerkin and least squares solution of first order elliptic systems. In particular, optimal order error estimates for piecewise polynomial approximation spaces were derived. These estimates were available only under certain conditions on the approximating spaces. The purpose of this paper is to illustrate the theory of the previous papers by providing numerical examples and to furnish examples of grids which do and do not satisfy the above conditions necessary for optimal convergence.

---

*Department of Mathematics, Carnegie-Mellon University, Pittsburgh, PA

†Department of Mathematics, University of Tennessee, Knoxville, TN

#ICASE, NASA Langley Research Center, Hampton, VA

This paper was prepared as a result of work performed under NASA Contract Number NAS1-14101 at ICASE, NASA Langley Research Center, Hampton, VA 23665.

I. Introduction

The first two papers in this series developed an abstract theory for the approximation of elliptic boundary value problems using mixed variational principles. It was shown that optimal approximations will result if and only if a grid decomposition property (hereafter G.D.P.) held. This paper reports numerical results verifying the theory.

An interesting feature of G.D.P. is that its validity requires conditions on the grids entering into the definition of finite element spaces. A secondary purpose of this paper is to furnish examples of grids which satisfy G.D.P. and grids which do not. For example, in the case of second order elliptic problems where linear elements are used, we prove that the "criss-cross grid" (see Figure 2-2b) does satisfy the G.D.P.

II. Numerical Results for the Least Squares Principle

In this section we report the results of computations which illustrate the least squares method discussed in [2]. These results give evidence of the essential role played by the G.D.P. Furthermore, they point out certain advantages that the least squares method possesses over the use of either the Dirichlet or Kelvin variational principles.

All the examples deal with the Helmholtz equation

$$\Delta\phi + k^2\phi = F(x,y) \tag{1}$$

in the unit square. An equivalent first order system is given by

$$\operatorname{div} \underline{u} + k^2\phi = F(x,y) \tag{2}$$

and

$$\underline{u} - \operatorname{grad} \phi = 0 \tag{3}$$

Three different sets of boundary conditions were used; these are depicted in Figure 2-1. In conjunction with these data, three different grids were used; these are illustrated in Figure 2-2. The grids of Figure 2-2a and 2-2b lead to two different piecewise linear finite element spaces, while the grid of Figure 2-2c leads to a piecewise bilinear finite element space.

Sample computational results are presented in Figures 2-3 to 2-6. Figure 2-3 displays the L_2 error of the approximate solution for the components u and v of grad ϕ. The exact solution is $\phi = \sin(x-y)$. Both the Dirichlet and Neumann problems for (2) - (3) were computed for the three grids of Figure 2-2 with $k = 1/2$. In these cases, u and v have identical errors. Next the mixed data case of Figure 2-1c was considered. In this case, the exact solution of the problem is given by

$$\phi = \cos(\pi y)\ \cos\left[\sqrt{\pi^2-k^2}\,(1-x)\right] \Big/ \cos\left(\sqrt{\pi^2-k^2}\right) .$$

Figure 2-4 displays the L_2 errors in u and v for the "directional" and "criss-cross" grids, again with $k = 1/2$. For the "criss-cross" grid, results are also given for $k = 7/4$ in which case (1), or equivalently

(2) - (3), is indefinite. In all the above examples, the approximating spaces were constrained to satisfy the appropriate essential boundary conditions. An alternative approach is to leave the approximating spaces unconstrained, and instead include the essential boundary conditions in the variational principle [3]. Figure 2-4 also displays results for the latter approach, using the "criss-cross" grid for both $k = 1/2$ and $7/4$. Figure 2-5 displays the L_2 errors in ϕ using the "criss-cross" grid with $k = 1/2$ and $7/4$ and using both methods of imposing the boundary conditions on the approximate solution. Finally, in Figure 2-6, results for other examples using the "criss-cross" grid are presented. For contrast, one result is given using the "directional" grid.

The results of these and other computations may be summarized as follows. For all problems considered, the "criss-cross" grid yielded a second order rate of convergence for the approximations to ϕ, u and v. Although the "directional" and bilinear grids generally yielded a second order rate of convergence for the approximations to ϕ, they generally did not achieve such a rate for u and v. These results clearly point out the crucial role the choice of grid plays in achieving an optimum rate of convergence of the approximations to $\underline{u}$. Furthermore, at least for u and v, the "criss-cross" grid consistently yielded smaller values for the L_2 errors, even at moderately large values of the grid size. It is shown in Section 4, which deals with the G.D.P., that the "criss-cross" grid satisfies this property.

Unlike the Dirichlet or Kelvin principles, the least squares principle allows the use of similar spaces for approximating the scalar ϕ and vector $\underline{u}$. The Kelvin principle requires that the space in which one seeks the approximation to ϕ be formed as the divergence of the elements of the space in which one seeks approximations to $\underline{u}$ [1]. Analogously, the

Dirichlet principle implicitly requires that the space in which one seeks approximations to $\underline{u}$ be composed of the gradient of the elements of the scalar approximating space. Thus, these two principles excluded the possibility of using, for instance, continuous piecewise linear finite element spaces for both ϕ and $\underline{u}$. Therefore one cannot, in general, simultaneously achieve second order accuracy in the approximations to ϕ and $\underline{u}$. The least squares principle does not require any such inclusion property and one may choose piecewise linear spaces for the approximations to ϕ and $\underline{u}$. Therefore as is shown in [2] and illustrated in the examples of this section, one may achieve second order accuracy in both the approximations to ϕ and $\underline{u}$. Of course, actually achieving the second order accuracy in approximations to $\underline{u}$ requires that the grid be chosen so that the G.D.P. be satisfied. This fact was proved in [2]. The optimal accuracy of approximations to ϕ, however, is independent of this grid requirement.

A final comment on the least squares method concerns the fact that the matrix system resulting from the discretization is symmetric and positive definite. These desirable matrix properties remain valid even if the problems associated with (1) or (2)-(3) are indefinite, e.g. k^2 in (1) or (2)-(3) is larger than the magnitude of the smallest (in modulus) eigenvalue of the Laplacian operator. The same will not be true for the Dirichlet or Kelvin principles. Thus, even for indefinite problems, the least squares method allows for the use of standard iterative techniques for the solution of the associated matrix problem. In fact, insofar as the properties of the least squares method discussed in [2] and in this paper are concerned, the method is insensitive to the value of k except, of course, for the near singular cases where k^2 approaches an eigenvalue of the Laplacian operator. Furthermore, the least squares method of [2] results in a matrix which has a zero-nonzero structure identical to that of the matrix obtained by using the Kelvin principle with an identical choice of approximation spaces.

III. Numerical Results for the Kelvin Principle

In this section we briefly report the results of computations based on the Kelvin principle discussed in [1]. These results give further evidence of the essential role played by the G.D.P. The examples of this section deal with the Poisson equation [(1) of section 2 with $k = 0$]. An equivalent first order system is given by (2)-(3) of section 2 with $k = 0$.

We first consider results for the mixed data problems depicted in Figure 2-1c using the "directional" grid illustrated in Figure 2-2a. The particular problem considered has an exact solution given by

$$\phi = \sin(\pi x/2)\cos(\pi y) \quad . \tag{1}$$

Figure 3-1 displays the L_2 error of the approximate solution for ϕ and the components u and v of $\underline{u} = \text{grad}\ \phi$. The figure indicates that the L_2 errors in u and v remains roughly constant and the L_2 error in ϕ grows linearly as the size of the grid is reduced. We recall from [1] that the G.D.P. is necessary and sufficient for the stability of the Kelvin approximation. The results shown in Figure 3-1 indicate that the "constant" C_G appearing in the definition of the G.D.P. in fact grows like h^{-2}, where h is a measure of the grid size. As a result, all accuracy in the approximation to $\underline{u}$ is lost, and the approximation in ϕ actually becomes unbounded. These results, and those below concerning the criss-cross grid give further evidence of the importance of the G.D.P.

The directional grid used to generate the results of Figure 3-1 does not satisfy the G.D.P. However, Lemma 1 of [1] is independent of this property of the grid. In the context of the directional grid, that

lemma shows that the divergence of the error in the approximation to $\underline{u}$ should be $0(h)$. This result is confirmed in Figure 3-1 where that divergence is graphed as a function of h. As is evident from the figure, the divergence of the error in $\underline{u}$ is indeed $0(h)$ even though the error in $\underline{u}$ itself is $0(1)$.

We now consider results using the "criss-cross" grid illustrated in Figure 2-2b. Figure 3-2 displays the L_2 errors of the approximate solutions for u and v. Results are given for the mixed data problem with exact solution given by (1) and for a Dirichlet problem with exact solution

$$\phi = \sin(\pi x)\sin(\pi y) \quad .$$

The mixed data and Dirichlet problems were approximated using an evenly spaced grid. In addition, computations for the mixed data problem were carried out using a variable grid whose spacing is determined by choosing an even spacing in a (ξ,η) coordinate system, and then letting

$$x = \xi^3 \qquad \text{and} \qquad y = \eta^3 \quad .$$

This stretching has the effect of accumulating grid points near $x = 0$ and $y = 0$. For all cases, the computed rate of convergence, using criss-cross grids, is of second order. The results shown in Figure 3-2, especially when compared with those of Figure 3-1 for the directional grid, are lucid evidence of the necessity of the G.D.P. to the achievement of optimal orders of accuracy.

IV. Proof that the Criss-Cross Grid Satisfies the G.D.P.

For simplicity consider the Dirichlet problem for the uniform grid shown in Figure 2-2b with $\underline{V}_0^h = \underline{V}^h$ being the space of $\mathbb{R}^2$ - valued piecewise linear functions. To verify that this grid satisfies the G.D.P. we must show that there is a positive number

(1) $$0 < C_G < \infty$$

independent of h for which the following holds. Given any

(2) $$f_h \in S^h = \mathrm{div}(\underline{V}^h)$$

there is a v_h in $\underline{V}^h$ for which

(3) $$\mathrm{div}(\underline{v}^h) = f_h$$

and

(4) $$\| \mathrm{div}(\underline{v}^h) \|_0 \leq \| f_h \|_{-1}$$

The first step is to construct a local basis for $\underline{V}^h$. The verification will be completed by showing (3)-(4) holds for each element f_h of this basis.

Since $\underline{V}^h$ consists of piecewise linear functions on the grid in Figure 2-2b, observe that (2) implies that each f_h in S^h is a piecewise constant function. What is interesting is that S^h is a strict subspace of the space $\hat{S}^h$ of all piecewise constant functions on the criss-cross grid in Figure 2-2b. Indeed, the following gives a rule for determining when a function f_h in $\hat{S}^h$ is actually in S^h.

Lemma 1: Let f_h be in $\hat{S}^h$. Then f_h is in S^h iff the following holds. Given any rectangle R containing triangles T_1, T_2, T_3, T_4 (see

Figure 4-1) it is true that

$$f_h(T_1) + f_h(t_3) = f_h(T_2) + f_h(T_4) \tag{5}$$

where $f_h(T_j)$ is the value of f_h in T_j.

The proof of Lemma 1 will follow from Lemma 2 stated and proved below.

Note that since the dimension $\dim(\hat{S}^h)$ of $\hat{S}^h$ is equal to the number m of triangles in the grid, it follows from (5) that

$$\dim S^h = 3m/4 \ . \tag{6}$$

Moreover, a locally defined basis can be constructed as follows. For each rectangle R (see Figure 4-1) we associate three functions ψ_1,ψ_2,ψ_3 which vanish outside R. The piecewise constant function ψ_i is uniquely determined in R by the requirement that it is identically 1 in $T_i \cup T_{i+1}$ and zero in the other two triangles in R. As R varies over all rectangles this process defines $3m/4$ independent functions in S^h and hence the set of such functions is a basis for S^h. Interestingly, this basis is exactly the union of the basis for piecewise constant functions for the two directional grids shown in Figure 4-2.

Lemma 1 follows as an easy consequence of our next Lemma, which in effect relates the components of any $\underline{v} \in \underline{V}^h$ satisfying $\mathrm{div}(\underline{v}) = f \in S^h$ to the value of f. Before stating and proving this lemma it is convenient to first introduce a new coordinate system. For the generic rectangle R of Figure 4-1 let σ_i and τ_i denote the components of $\underline{v}(P_i)$ $(1 \leq i \leq 4)$ along the diagonals, and let ξ_0 and η_0 be the analogous components of $\underline{v}(P_0)$. (See Figure 4-3.) Then the condition that $\mathrm{div}(\underline{v}) = f$ in R constrains only certain components of $\underline{v}$. The coupling is shown in Figure 4-4, with the precise relations given in the following lemma.

Lemma 2. Let f be a piecewise constant function on the rectangle R with δ_i denoting the value of f on the triangle T_i $(i = 1,2,3,4)$. Then there is a continuous $\mathbb{R}^2$ valued function $\underline{v}$ which is linear in each triangle T_i and which satisfies

$$\operatorname{div}(\underline{v}) = f \quad \text{in} \quad R \tag{7}$$

if and only if

$$\delta_1 + \delta_3 = \delta_2 + \delta_4 \quad . \tag{5'}$$

Assuming the truth of Lemma 2, the rotated coordinates (σ_i,τ_i) of $\underline{v}$ at the point P_i $(i = 1,2,3,4)$ satisfy

$$\sigma_1 = \sigma_3 + \tau_2 - \tau_4 + (\delta_1+\delta_2)h/\sqrt{2} \quad . \tag{8}$$

In addition, the (rotated) coordinates (ξ_0,η_0) of $\underline{v}(P_0)$ satisfy

$$2\xi_0 = 2\sigma_1 + \tau_4 - \tau_2 - (\delta_1+\delta_2)h/\sqrt{2} \tag{9}$$

$$2\eta_0 = \tau_4 + \tau_2 - (\delta_1-\delta_2)h/\sqrt{2} \tag{10}$$

Conversely, if (5'), (8)-(10) hold, then so does (7).

Let us momentarily postpone the proof of Lemma 2 and turn to our basic problem of verifying the G.D.P. First, observe that it is sufficient to verify (4) for the case where $f_h = \psi$, an arbitrary member of the local basis. To estimate

$$\| \psi \|_{-1} \tag{11}$$

we solve the Dirichlet problem

$$\Delta\phi = \psi \quad \text{in} \quad \Omega \quad , \qquad \phi = 0 \quad \text{on} \quad \Gamma \tag{12}$$

Then (11) is equal to $\| \nabla \phi \|_0$. Thus, if $G(\underline{x},\underline{y})$ denotes the Green's function for this problem, we have

$$\phi(\underline{x}) = \int_{\Omega} G(\underline{x},\underline{y})\psi(\underline{y})d\underline{y}$$

But ψ is equal to zero except on two triangles, call them T_1 and T_2, where ψ is identically 1. Hence

$$\phi(\underline{x}) = \int_{T_1 \cup T_2} G(\underline{x},\underline{y})d\underline{y} \ ,$$

and so

$$(\nabla\phi)(\underline{x}) = \int_{T_1 \cup T_2} \nabla_{\underline{x}} G(\underline{x},\underline{y})d\underline{y} \ .$$

It follows that

$$\| \psi \|_1 \geq C_1 h^2$$

for some positive constant C_1 independent of ψ and h. Our task is therefore to find a piecewise linear $\underline{v}$ such that

$$\text{div}(\underline{v}) = \psi \tag{13}$$

and

$$\| \underline{v} \|_0 \leq C_2 h^2 \tag{14}$$

for some positive constant C_2 independent of $\underline{v}$, ψ and h. If this holds the C_G can be any number greater or equal to C_2/C_1.

As is evident from Lemma 2 there are many $\underline{v} \in \underline{V}^h$ satisfying (13). Moreover, as we shall see momentarily all will have nodal values of order

$O(h)$ near the triangles T_1 and T_2 where ψ is 1. However, the crucial step in our construction is to show $\underline{v}$ can be chosen such that its nodal values decrease exponentially as we move away from $T_1 \cup T_2$ (roughly by a factor of two for each mesh spacing). This property yields (14). Interestingly, the exponential decay does not occur for either of the directional grids in Figure 4-2.

Suppose ψ is 1 in the shaded triangles shown in Figure 4-5 and is zero elsewhere. For simplicity we order the vertices of the subrectangles as shown in this Figure, and let

$$\sigma_{ij} = \hat{\sigma}_{ij} h/\sqrt{2} \quad , \quad \hat{\tau}_{ij} = \tau_{ij} h/\sqrt{2} \tag{15}$$

denote the rotated coordinates σ,τ of $\underline{v}$ at the (i,j) node. In addition, we let

$$\xi_{ij} = \hat{\xi}_{ij} h/\sqrt{2} \quad , \quad \eta_{ij} = \hat{\eta}_{ij} h/\sqrt{2} \tag{16}$$

denote the coordinates of $\underline{v}$ at the midpoints (see Figure 4-6).

The couplings between (15)-(16) are given in Lemma 2. In particular, for the rectangle containing the shaded triangles we have from (8) (with $\delta_1 = \delta_4 = 1$)

$$\hat{\sigma}_{11} = \hat{\sigma}_{00} + \hat{\tau}_{10} - \hat{\tau}_{01} + 1 \tag{17}$$

$$2\hat{\xi}_{11} = 2\hat{\sigma}_{11} - \hat{\tau}_{10} + \hat{\tau}_{01} - 1 \tag{18}$$

$$2\hat{\eta}_{11} = \hat{\tau}_{10} + \hat{\tau}_{01} - 1 \tag{19}$$

For all other values of (i,j) we have

$$\hat{\sigma}_{i+1,j+1} = \hat{\sigma}_{ij} + \hat{\tau}_{i+1,j} - \hat{\tau}_{i,j+1} \tag{20}$$

(21) $$2\hat{\xi}_{ij} = 2\hat{\sigma}_{i+1,j+1} - \hat{\tau}_{i+1,j} + \hat{\tau}_{i,j+1}$$

(22) $$2\hat{\eta}_{ij} = \hat{\tau}_{i+1,j} - \hat{\tau}_{i,j+1}$$

First we set

$$\hat{\sigma}_{ij},\ \hat{\tau}_{ij},\ \hat{\xi}_{ij},\ \hat{\eta}_{ij}$$

to zero whenever either i or j are negative. Observe from the above that $\hat{\sigma},\hat{\tau}$ can be computed from (17) and (20) independently of the values $\hat{\xi},\hat{\eta}$ at the midpoints of the rectangles. Moreover, (17), (20) define recurrence relations for $\hat{\sigma}_{i+1,j+1}$ along the lines

(23) $$i - j = \text{constant}$$

The idea is to select $\hat{\tau}_{ij}$ such that $\hat{\sigma}_{ij}$ decreases by a factor of two as we move along (23) for increasing i. Indeed, the solution which has this property is illustrated in Figure 4-7 and is defined as follows. Along the line

(24) $$i - j = 0$$

$\hat{\sigma}_{ij}$ is equal to 2^{-i+1} for $i \geq 1$. It is zero for $i \neq j$. The orthogonal component $\hat{\tau}_{ij}$ is constant in magnitude along the lines

(25) $$i + j = \text{constant}.$$

When $i + j$ is even, $\hat{\tau}_{ij}$ is zero. When it is odd, say

(26) $$i + j = 2k-1 \ ,$$

then

(27) $$\hat{\tau}_{ij} = \pm \tfrac{1}{2} k \ ,$$

the plus sign belonging to points where $j > i$ and the minus sign belonging to points where $j < i$.

It is not necessary to work out the values of $\hat{\xi}_{ij}$, $\hat{\eta}_{ij}$. Indeed, it is clear from (21)-(22) that these also decrease exponentially as we move away from the node $(0,0)$. This completes our construction of the $\underline{v} \in \underline{V}^h$ satisfying (13)-(14).

It remains to prove Lemma 2, and to do this we use the relation

$$\int_T \operatorname{div}(\underline{v}) = \int_{\partial T} \underline{v}\cdot\underline{\nu} \quad , \tag{28}$$

where T is any triangle and $\underline{\nu}$ is the outer normal to T. Since $\underline{v}$ is piecewise linear (28) reduces to

$$h \operatorname{div}(v) = \sum_{i=1}^{3} (\underline{v}\cdot\underline{\nu})(m_i) \quad , \tag{29}$$

where m_1, m_2, m_3 are the midpoints of the three sides of T. Suppose we are given the generic rectangle R (see Figure 4-4) with δ_i being the value of $f = \operatorname{div}(\underline{v})$ in T_i. Moreover, let (σ_i,τ_i), (ξ_0,η_0) be the (rotated) coordinates of $\underline{v}(P_i)$ as in Figure 4-3. Then applying (29) to T_1 gives

$$\sigma_1 + \tau_4 - \xi_0 - \eta_0 = \delta h/\sqrt{2} \tag{30}$$

Similar applications to T_2, T_3, and T_4 give

$$\sigma_1 - \tau_2 - \xi_0 + \eta_0 = \delta_2 h/\sqrt{2} \tag{31}$$

$$\tau_4 - \sigma_3 + \xi_0 - \eta_0 = \delta_4 h/\sqrt{2} \tag{32}$$

$$-\tau_2 - \sigma_3 + \xi_0 + \eta_0 = \delta_3 h/\sqrt{2} \tag{33}$$

It follows that

$$\delta_1 + \delta_3 = \delta_2 + \delta_4 \tag{34}$$

is necessary and sufficient for these two equations to have a solution. Moreover, if (34) holds then (30)-(33) can be recombined as (8)-(10).

REFERENCES

[1] Fix, George J., Gunzburger, Max D., and Nicolaides, R. A.: "On Mixed Finite Element Methods: I. The Kelvin Principle." ICASE Report No. 77-17 (1977). To appear in Numerische Mathematik.

[2] Fix, George J., Gunzburger, Max D., and Nicolaides, R. A.: "On Mixed Finite Element Methods: II. The Least Squares Method." ICASE Report No. 77-18 (1977). To appear in Numerische Mathematik.

[3] Bramble, J. H. and Schatz, A. H.: "Least Squares Method for 2mth-Order Elliptic Boundary-Value Problems," Math. Comp. 25 (1971), pp. 1-32.

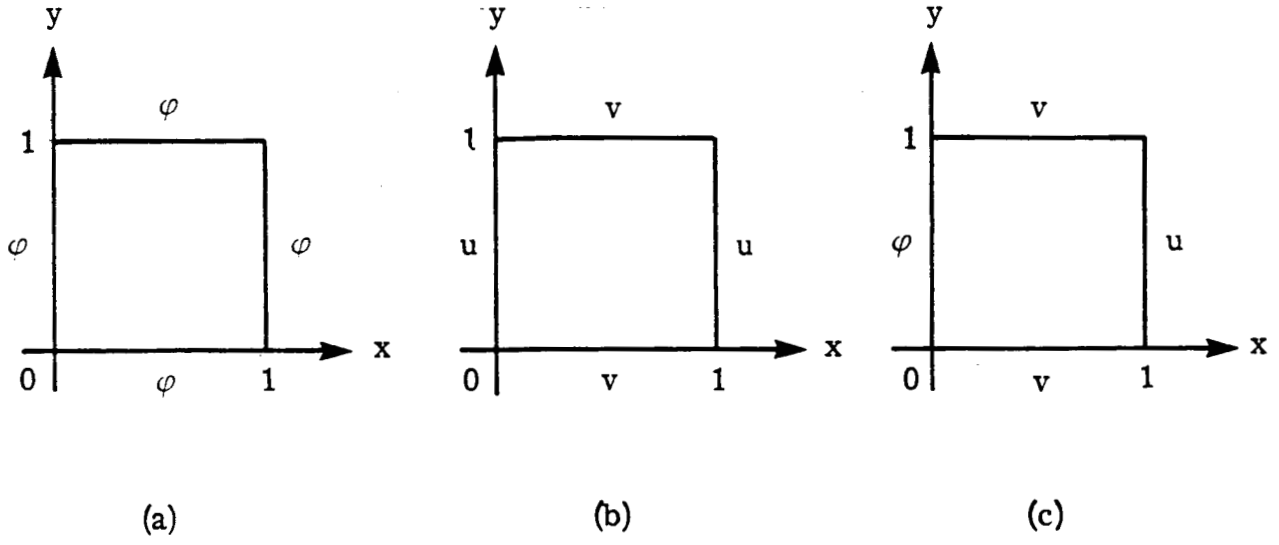

Figure 2-1. Different boundary value specifications used in numerical examples. Symbols indicate variable specified on corresponding section of boundary. a) Dirichlet data; b) Neumann data; c) Mixed data.

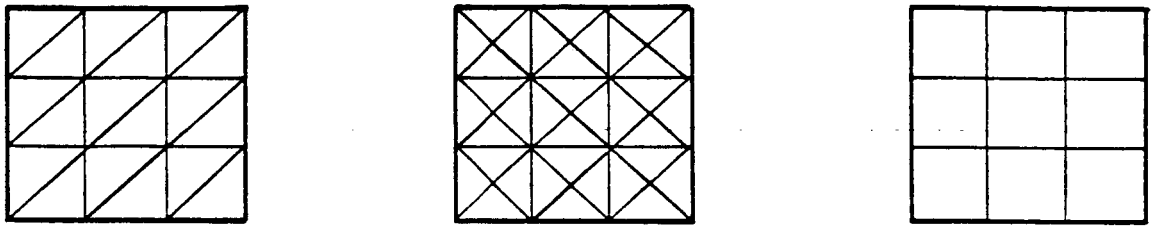

Figure 2-2. Grids used in numerical examples. a) "Directional" triangulation; b) "Criss-cross" triangulation; c) Bilinear quadrilaterals.

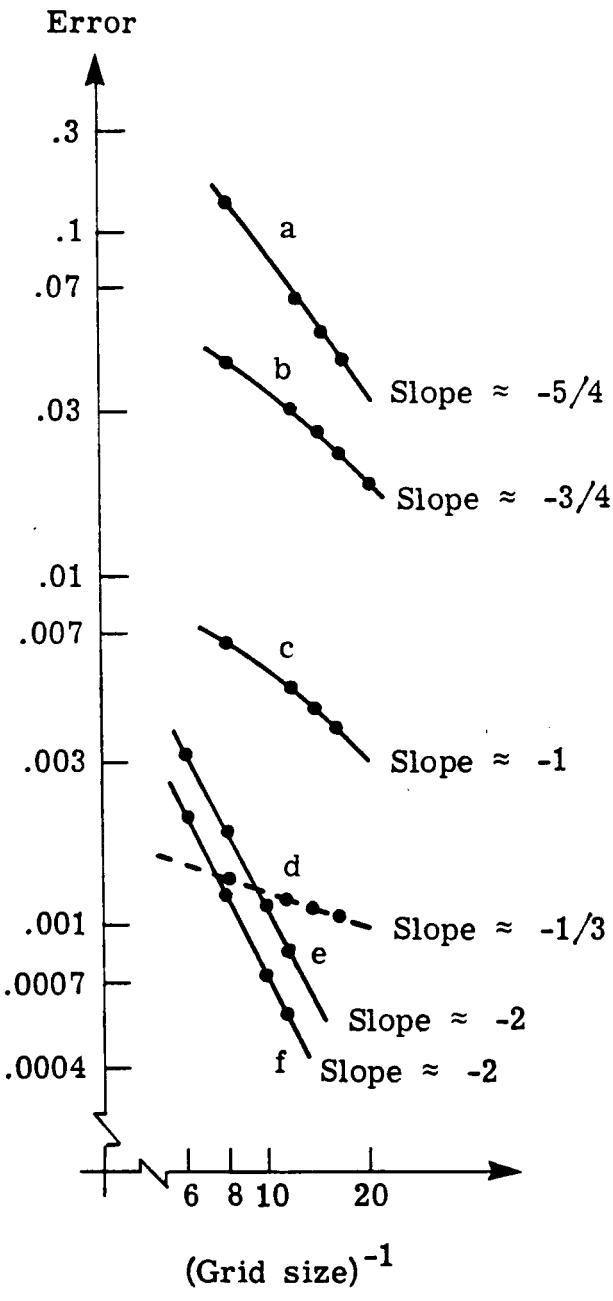

Figure 2-3. L_2 error in the least squares approximation to $u = \partial\phi/\partial x$ or $u = \partial\phi/\partial y$ for Dirichlet (a,b,f) and Neumann (c,d,e) problems with $k = \frac{1}{2}$. (b,d) directional grid; (a,c) bilinear grid; (e,f) criss-cross grid.

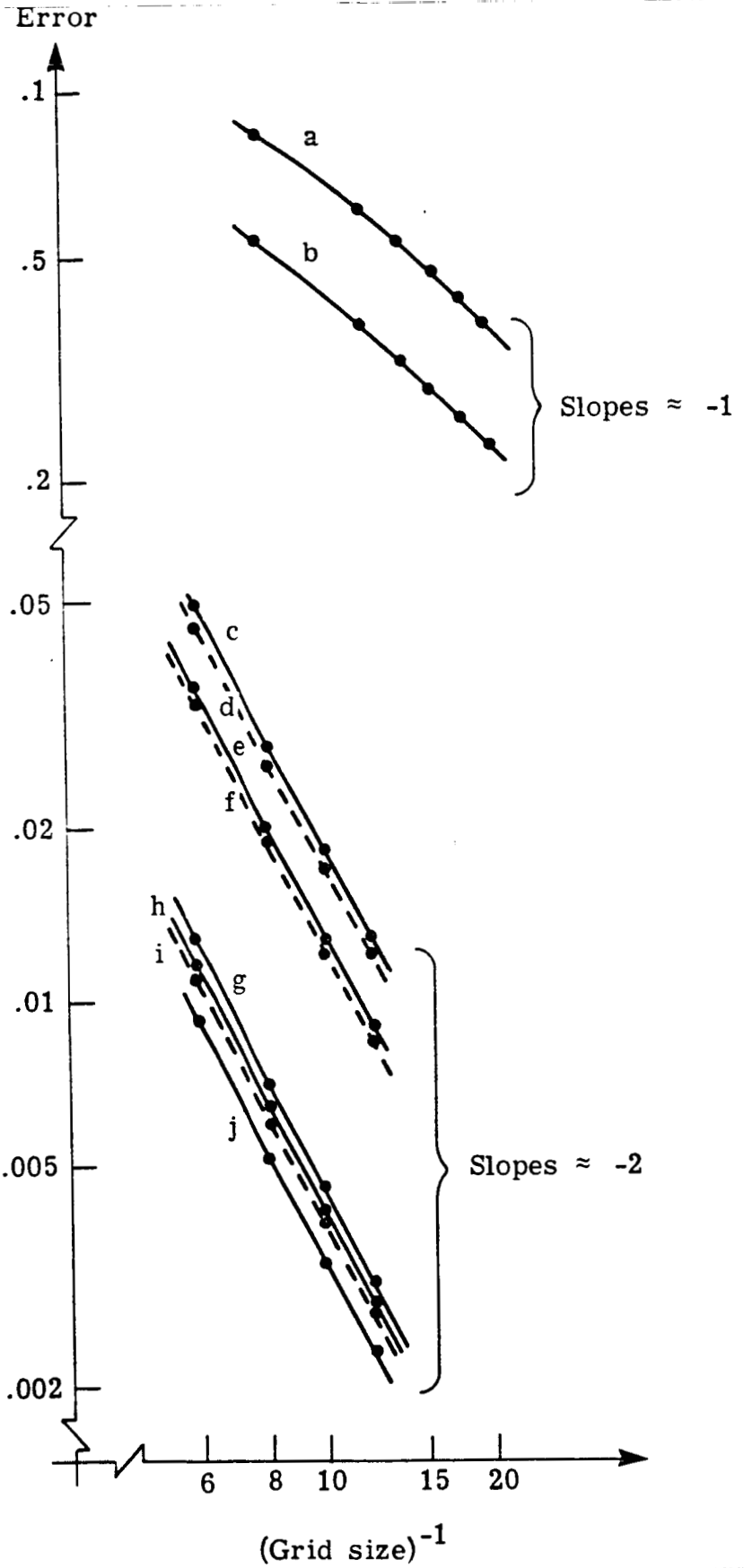

Figure 2-4. L_2 error in the least squares approximation to $u = \partial\phi/\partial x$ and $v = \partial\phi/\partial y$ for mixed boundary problem. (a,b) directional grid; (c-i) criss-cross grid. (a-f) $k = \frac{1}{2}$; (g-j) $k = 7/4$. (a,c,e,g,i) displays u; (b,d,f,h,j) displays v. (a-d,g,k) using constrained spaces; (e,f,i,j) using boundary integrals.

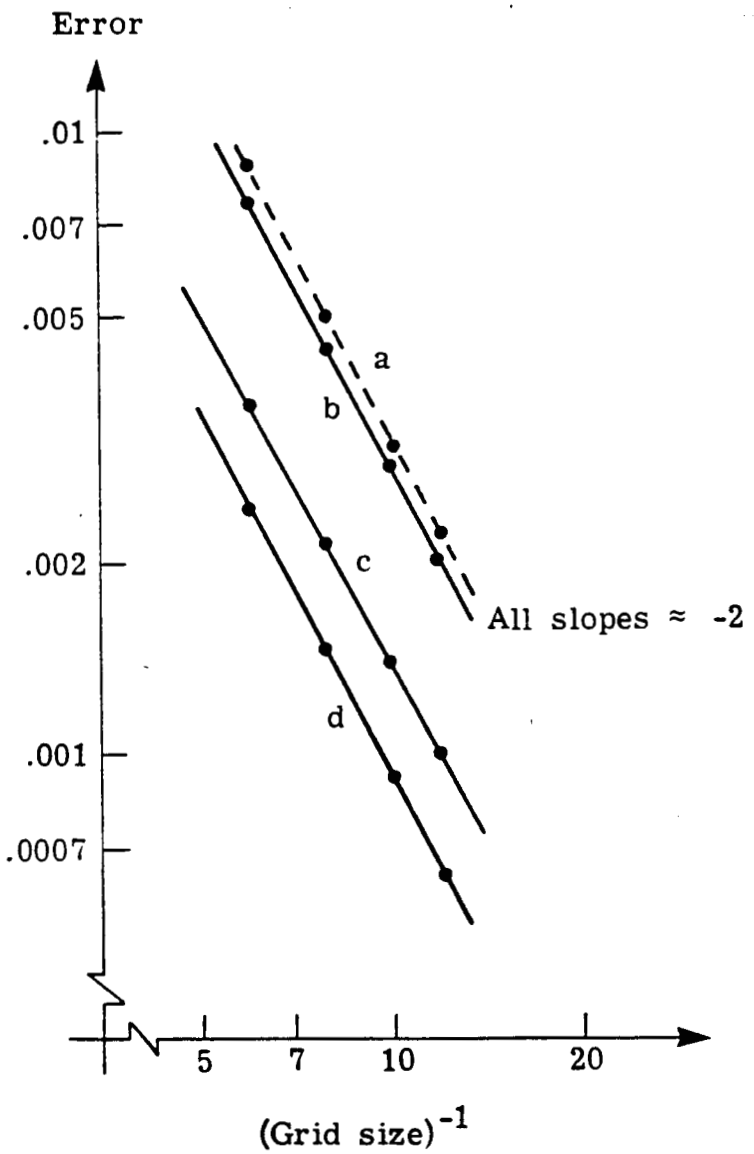

Figure 2-5. L_2 error in the least squares approximation to ϕ for mixed data problem using the criss-cross grid. (a,c) k = 7/4; (b,d) k = $\frac{1}{2}$. (a,b) using boundary integrals (c,d) using constrained spaces.

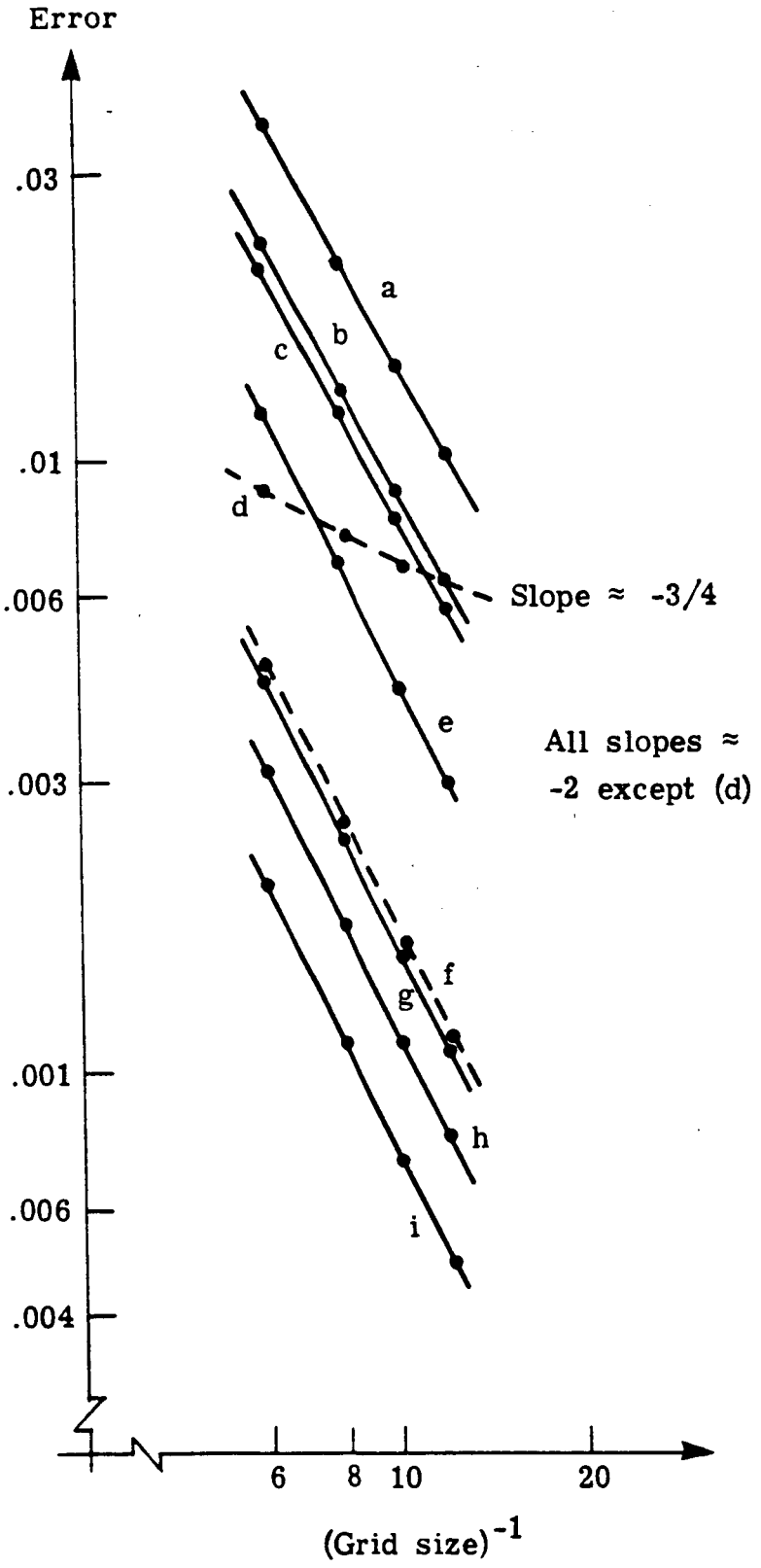

Figure 2-6. L_2 error in the least squares approximation to $u = \partial\phi/\partial x$ and $v = \partial\phi/\partial y$ using the criss-cross grid (except for d which uses the directional grid) with $k = \frac{1}{2}$. (a,c,d,f,g,h,i) displays u; (a,b,d,e,f,g,i) displays v. (a,b,c,d,) Dirichlet problem; (d,e,f,g,h) Neumann problem. (a,f) have exact solution $\phi = x^3 + y^3$; for (b,c,e,h) $\phi = \sin(2x-y)$; for (d,g,i) $\phi = \sin(xy)$.

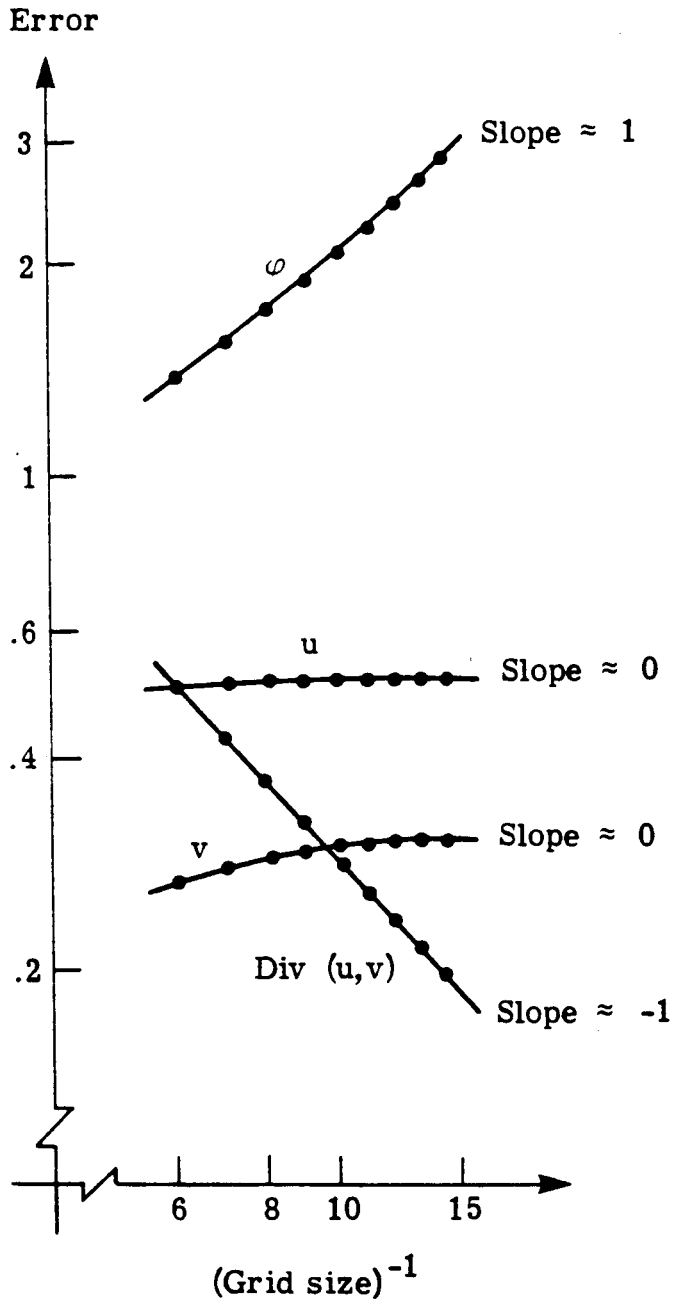

Figure 3-1. L_2 error in the Kelvin approximation to ϕ, $u = \partial\phi/\partial x$, $v = \partial\phi/\partial y$, and $div(u,v) = \partial u/\partial x + \partial v/\partial y$ using the directional grid for the mixed data problem.

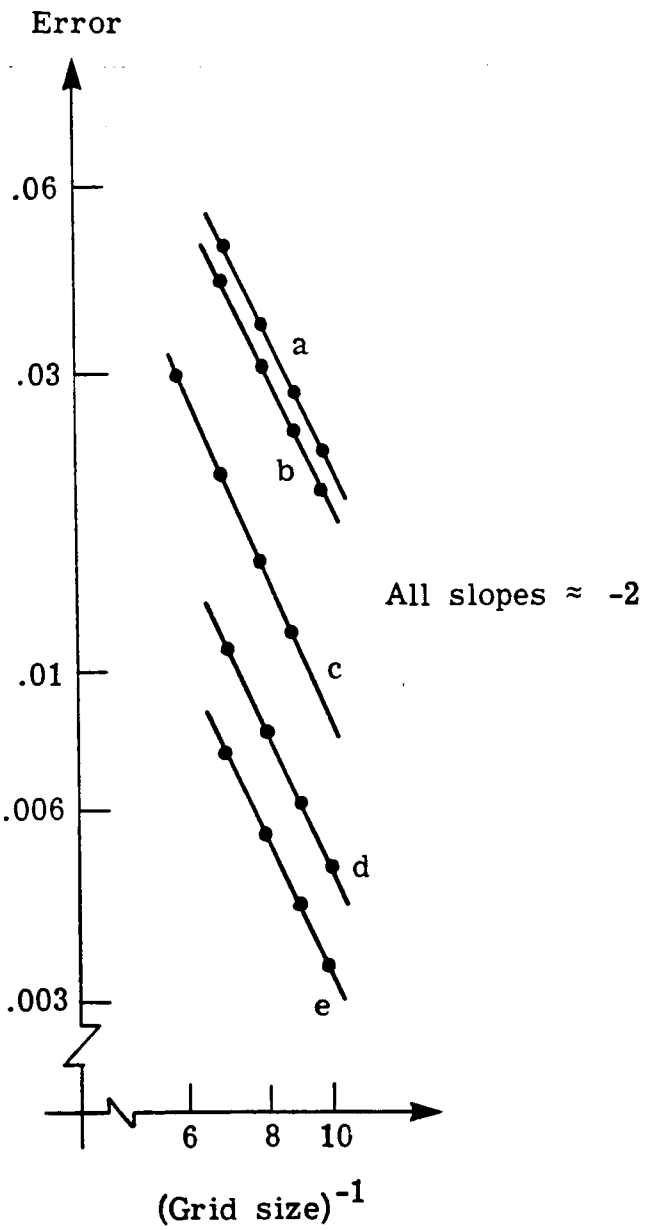

Figure 3-2. L_2 error in the Kelvin approximation to $u = \partial\phi/\partial x$ and $v = \partial\phi/\partial y$ using the criss-cross grid. (a,c,d) displays u; (b,c,e) displays v. (a,b) mixed data problem using a variable grid; (c) Dirichlet problem using a regular grid; (d,e) mixed data problem on a regular grid.

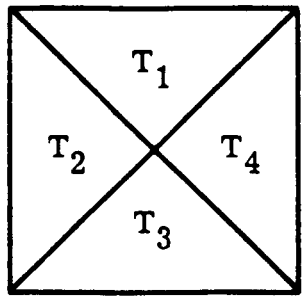

Figure 4-1. The generic rectangle R.

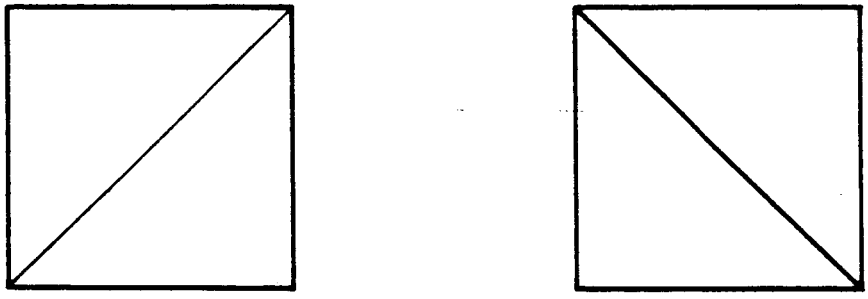

Figure 4-2. Directional grids.

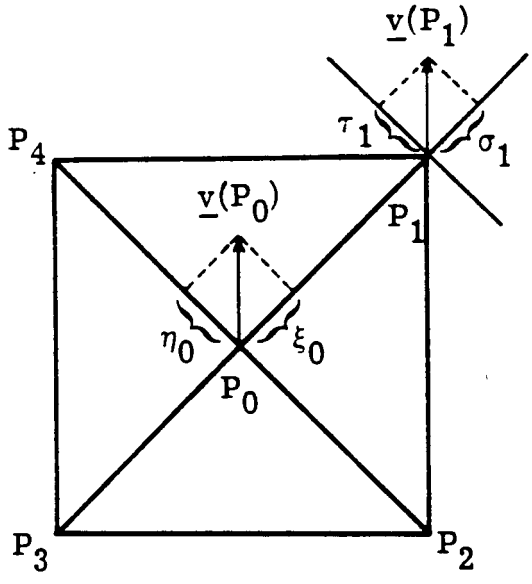

Figure 4-3. Rotated coordinates.

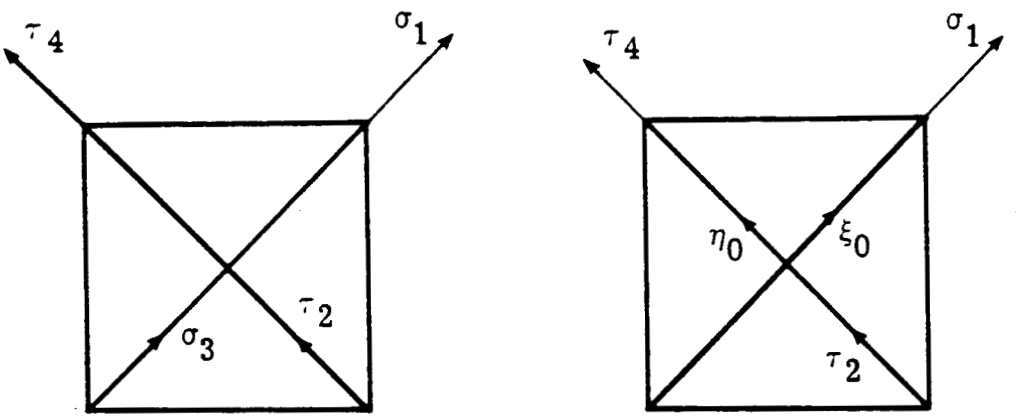

Figure 4-4. Couplings induced by the divergence condition (3).

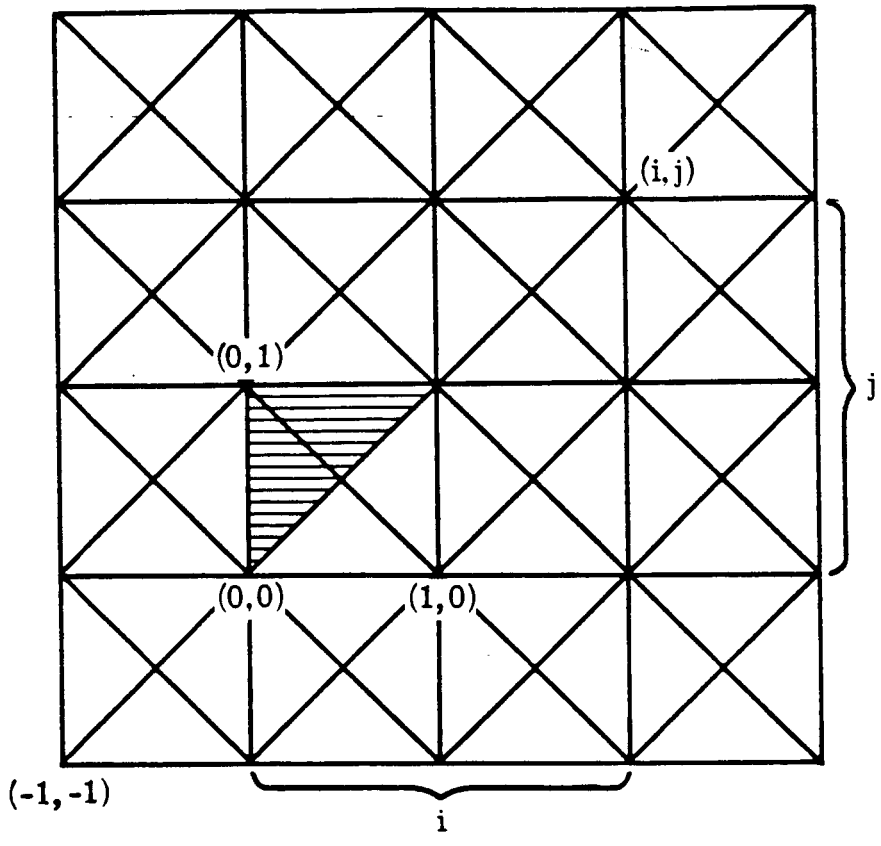

Figure 4-5. Support of the function ψ (shaded area).

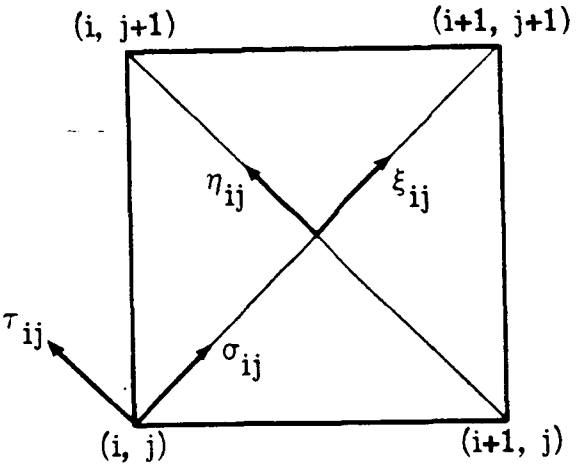

Figure 4-6. Coordinate labels.

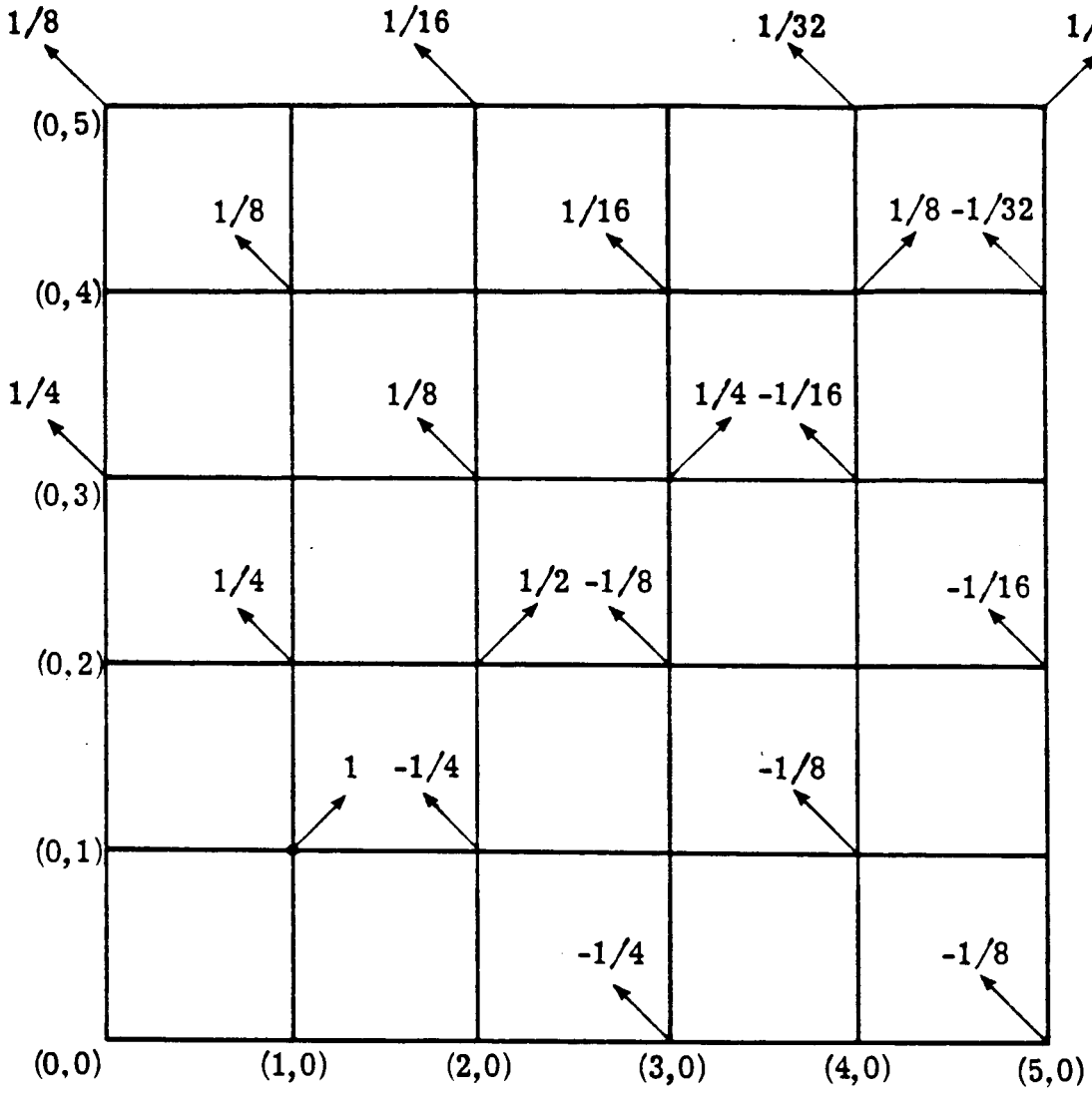

Figure 4-7. Nonzero values of $\hat{\sigma}_{ij}$ and $\hat{\tau}_{ij}$.